

ON THE BARYONIC CONTENTS OF LOW MASS GALAXIES

NICKOLAY Y. GNEDIN^{1,2,3}
Draft version February 27, 2018

ABSTRACT

The baryonic Tully-Fisher relation is an important observational constraint on cosmological and galactic models. However, it is critical to keep in mind that in observations only stars, molecular, and atomic gas are counted, while the contribution of the ionized gas is almost universally missed. The ionized gas is, however, expected to be present in the gaseous disks of dwarf galaxies simply because they are exposed to the cosmic ionizing background and to the stellar radiation that manages to escape from the central regions of the galactic disks into their outer layers. Such an expectation is, indeed, born out both by cosmological numerical simulations and by simple analytical models.

Subject headings: galaxies: kinematics and dynamics – galaxies: dwarf – galaxies: irregular – galaxies: spiral – methods: numerical

1. INTRODUCTION

The baryonic Tully-Fisher relation (BTFR; Freeman 1999; McGaugh et al. 2000) extends the classical Tully-Fisher relation (Tully & Fisher 1977) by including, in addition to stars, all the baryonic content of galaxies. The physical reason for such an extension is very sound - in galactic halos that maintain the universal fraction of baryons, the baryonic mass becomes a linear proxy of the total mass. A deviation from the expected total mass - rotational velocity relation may indicate missing baryons (although such deviations may be degenerate with the effect of stellar feedback, e.g. Dutton & van den Bosch 2009); hence baryonic Tully-Fisher relation becomes a powerful test of galaxy formation models.

It is not surprising, therefore, that a significant effort has been expended over the years in measuring the BTFR in a diverse set of galaxies (Verheijen 2001; Bell & de Jong 2001; Gurovich et al. 2004; McGaugh 2005; Pfenniger & Revaz 2005; Begum et al. 2008; Stark et al. 2009; Trachternach et al. 2009; Gurovich et al. 2010; Torres-Flores et al. 2011). The current state of affairs is well synthesized by McGaugh (2011). The remarkable power-law behavior of BTFR over 4 decades in mass indicates a substantial fraction of “missing” baryons in the lowest mass galaxies. The observed “baryonic” components of these galaxies are dominated by atomic gas, and the decreasing “baryonic” fraction with galaxy mass is often interpreted as a substantial mass loss from the dwarf galaxies.

A limitation of such an argument, however, is that no observation actually measures the *baryonic* contents of galaxies; only stars, molecular, and atomic gas are accounted in observational studies, but not the ionized gas (with a handful of exceptions). In other words, in dwarf, HI dominated galaxies, the observed BTFR is, in fact, an HI Tully-Fisher relation. One needs, therefore, be careful to distinguish the total BTFR that accounts for all of the baryons within the virial radius of a galaxy, and the observed BTFR that only includes stars and molecular and atomic gas, but does not account for the ionized

gas.

In this paper I demonstrate that dwarf galaxies are expected to contain warm ionized gas (to be distinguished from hot halos) - simply because the gaseous disks of galaxies are exposed to the cosmic background radiation (plus whatever of their own ionizing radiation escapes into the outer layers of their disks), which is going to ionize the outer layer of atomic disks down the column density $N_{\text{H}} \sim 10^{19} \text{ cm}^{-2}$, comparable to the transition column density between Lyman Limit systems (which are mostly ionized) and Damped Lyman- α systems (which are mostly neutral).

Hence, the interpretation of the observed BTFR is rather non-trivial, nor can it easily be used to deduce the fraction of baryons ejected by the feedback from dwarf galaxies.

2. SIMULATIONS

The simulation used in this paper is similar to the one described in Gnedin & Kravtsov (2010). Specifically, the Adaptive Refinement Tree (ART) code (Kravtsov 1999; Kravtsov et al. 2002; Rudd et al. 2008) is employed to model a $6h^{-1} \text{ Mpc}$ cube centered on a typical $2L_*$ (at $z=0$) galaxy. The Lagrangian region of a sphere with radius equal to $5R_{\text{vir}}$ at $z=0$ (a “region of interest”) is sampled in the initial conditions with the effective 512^3 resolution, while the rest of the simulation volume is sampled more crudely. This setup results in the mass resolution in the region of interest of $1.3 \times 10^6 M_{\odot}$ in dark matter. This region of interest is then allowed to refine adaptively as the simulation proceeds in a quasi-Lagrangian manner, all the way down to additional 6 levels of refinement (total spatial dynamic range of about 30,000), maintaining spatial resolution of 260 pc in comoving reference frame. The simulation adopts Λ CDM cosmology similar to the WMAP1 one ($\Omega_M = 0.3$, $\Omega_B = 0.046$, $\sigma_8 = 0.9$ and $h = 0.7$).

The physical processes modeled in the simulation are exactly the same as described in Gnedin & Kravtsov (2010), with one exception. In particular, the simulation incorporates gas cooling (including cooling on metals, molecular hydrogen, and dust), a phenomenological model for molecular hydrogen formation, full time-dependent and spatially variable 3D radiative transfer of ionizing and Lyman-Werner band radiation (both from local sources and from the incident cosmic background of Haardt & Madau (2001)) using the Optically Thin Variable Eddington Tensor (OTVET) approximation of

¹ Particle Astrophysics Center, Fermi National Accelerator Laboratory, Batavia, IL 60510, USA; gnedin@fnal.gov

² Department of Astronomy & Astrophysics, The University of Chicago, Chicago, IL 60637 USA

³ Kavli Institute for Cosmological Physics and Enrico Fermi Institute, The University of Chicago, Chicago, IL 60637 USA

Gnedin & Abel (2001), and star formation in the molecular gas using Krumholz & Tan (2007) recipe. The only difference from the Gnedin & Kravtsov (2010) simulation is that the supernova feedback is disabled.

Existing models of supernova feedback in cosmological simulations (and other types of stellar feedback, except the feedback from stellar ionizing radiation, that is explicitly included) are still insufficiently developed to be fully realistic. Therefore, I deliberately disable that form of feedback to limit numerical treatment to only those physical processes that can be modeled with a reasonable degree of realism.

It is difficult to envision that the supernova feedback would *increase* the baryonic mass of galaxies, hence baryonic fractions in model galaxies should be considered as upper limits on the baryonic fractions in a real universe; any reasonable stellar feedback models should reduce these fractions even further.

In order to verify that the results presented below are robust and numerically converged, I re-run the last 150 Myr of the time evolution in the simulation with an additional level of refinement (twice higher spatial resolution) and more aggressive refinement criteria (to enlarge the regions refined to the highest allowed level). This convergence test has demonstrated that all the results presented below are highly robust.

3. TOTAL AND OBSERVED BARYONIC TULLY-FISHER RELATIONS

In order to compare the simulation to the observations, the total baryonic mass (all the way to the virial radius) and the observed “baryonic” mass (i.e. the sum of the stellar mass, molecular gas mass, and atomic gas mass) are measured for all model galaxies from the region of interest. To measure the rotational velocity, the mass density profiles for various mass components of model galaxies are constructed, and the circular velocity V_f are measured at the radius containing 90% of all HI. This procedure is similar to the one adopted by McGaugh (2011). I have verified that, if the radius including either 80% or 95% of all atomic gas is used instead, the results would change by no more than a symbol size in Figure 1.

Since the region of interest is centered on a single large galaxy, only a handful of other noticeable isolated galaxies end up in that region by $z = 0$. To somewhat enlarge the sample, I show in Figure 1 both $z = 0$ and $z = 0.5$ simulation snapshots, which are apparently fully consistent with each other.

Figure 1 shows the two BTFR (the total baryonic one and the observed BTFR that only includes stellar mass, molecular gas mass, and atomic gas mass but not the ionized gas mass). The solid line tracks the best-fit observed BTFR (McGaugh 2011) relation in the form

$$M_{\text{bar}} = \frac{47 M_{\odot}}{(\text{km/s})^4} V_f^4.$$

The dotted line gives a relation between the product of the universal baryon fraction $f_{\text{uni}} = \Omega_B / \Omega_M$ and M_{200} (mass within the overdensity 200 with respect to the critical density) vs V_{max} for dark matter halos from Bolshoi and Multi-Dark simulations (Prada et al. 2011). This relation is slightly steeper than $f_{\text{uni}} M_{200} \propto V_{\text{max}}^3$ due to the halo concentration dependence on halo mass. The simulation lies to the right of that line in Figure 1 because V_{max} from pure N-body simulations is not a sufficiently accurate proxy for the disk circular velocity - halo contraction due to baryonic condensation results in $V_f \approx (1.2 - 1.3) V_{\text{max}}$.

It is also possible to estimate the HI masses of dark matter halos using abundance matching - i.e. identifying dark mat-

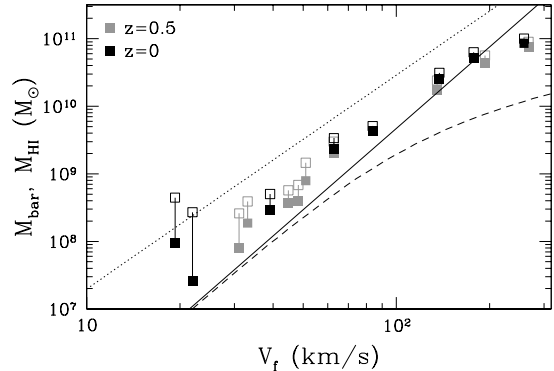


FIG. 1.— The baryonic Tully-Fisher relation for model galaxies at $z = 0$ (black) and $z = 0.5$ (gray); I show two redshifts since the $z = 0$ sample is very small by construction. Each model galaxy is represented by a vertical line with two symbols: open square shows the total baryonic mass of the galaxy; filled square shows the observed “baryonic” mass, i.e. the sum of stellar mass, molecular gas mass, and atomic gas mass. The difference between the two squares is the contribution of the ionized gas. The solid line is the best-fit observed BTFR from McGaugh (2011); the dotted line is $f_{\text{uni}} M_{200}$ vs V_{max} for dark matter halos in the Λ CDM cosmological model, while the dashed line is M_{HI} vs V_{max} obtained by abundance matching of the theoretical halo mass function and the observed HI mass function (see text for details).

ter halos from a theoretically computed halo mass function with HI galaxies from the actual observed HI mass function (Zwaan et al. 2005) that have the same spatial number density. The details on how this matching is performed are described in Marín et al. (2010) or Trujillo-Gomez et al. (2011); HI mass vs V_{max} that results from such abundance matching is shown in Fig. 1 with the dashed line. Not surprisingly, it matches the best-fit observed BTFR at low masses very well.

The observed BTFR in the simulation (solid squares) is not far from the best-fit line to the observational data, but is above it by about a factor of 2 for smallest galaxies. It is important to remember that the simulation should only be treated as an upper limit to the baryonic content of galaxies, because the stellar feedback is deliberately disabled in the simulation (except the feedback of ionizing radiation, which is included in the simulation by virtue of following the full spatially-variable and time-dependent 3D radiative transfer). The fact that the simulation points are not falling on the observed relation for $V_f \lesssim 200$ km/s simply illustrates the well-known fact that the stellar feedback processes are important for determining the baryonic contents of sub- L_* galaxies.

In order to illustrate the crucial difference between the total baryonic fraction and the observed (stars + molecular + atomic gas) baryonic fraction in model galaxies, I show the two fractions in Figure 2. As one can see, the total baryonic fraction in model galaxies remains close to universal all the way to $V_f \sim 40$ km/s, and at lower V_f the effect of photo-evaporation of gas from dark matter halos due to heating by the cosmic ionizing background radiation becomes important. That effect in this simulation is approximately described by a fitting formula of Gnedin (2000),

$$\frac{f_{\text{bar}}}{f_{\text{uni}}} = \left[1 + (2^{\alpha/3} - 1) \left(\frac{M_c}{M_{200}} \right)^{\alpha} \right]^{-3/\alpha} \quad (1)$$

with parameter values $\alpha = 1$ and $M_c = 7 \times 10^9 M_{\odot}$. The latter value is the same as found by Okamoto et al. (2008, converted from the virial overdensity of 97 with respect to the critical used there to the overdensity of 200 used here, for

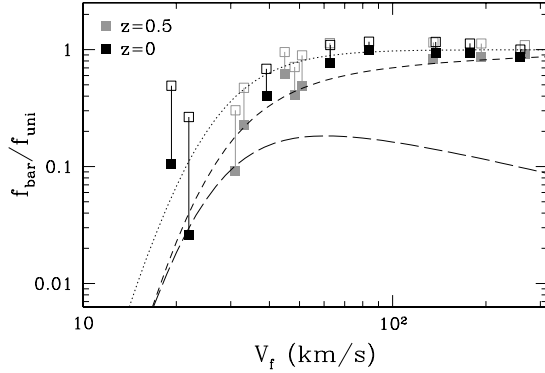


FIG. 2.— The baryonic fraction (in units of the universal fraction $f_{\text{uni}} = \Omega_B/\Omega_M$) for model galaxies at $z=0$ (black) and $z=0.5$ (gray). Symbols are the same as in Figure 1. The dotted line approximately traces the effect of photo-evaporation of gas from halos due to cosmic background (Equation 1) while the short-dashed line shows a simple model (3) for the neutral content of galactic disks in dwarf galaxies. The long-dashed line is the fraction of ionized gas within the HI radius (Equation 4). This function (plotted against V_{max}) is shown in Figure 2 as a dotted line. In agreement with McGaugh & Wolf (2010), this line alone is unable to explain the baryonic contents of dwarf galaxies.

It is also possible to construct a simple analytical model that approximately reproduces these results for the observed BTFR, following the ideas of Mo et al. (1998). Let's consider an exponential gaseous disk with the surface density run

$$\Sigma(R) = \Sigma_0 e^{-R/R_d},$$

such that the disk scale length is a given fraction μ of the halo virial radius R_{200} ,

$$R_d = \mu R_{200},$$

and the disk mass is a fraction ν of the total halo mass of M_{200} ,

$$2\pi\Sigma_0 R_d^2 = \nu M_{200},$$

so that

$$\Sigma_0 = \frac{\nu}{\mu^2} \frac{M_{200}}{2\pi R_{200}^2}$$

(expressions for μ and ν are given in Mo et al. (1998) as functions of other parameters). The disk is exposed to the cosmic ionizing background, which ionizes hydrogen (from both sides) in a slab of gas below the surface density Σ_{HII} . Then the mass of the neutral gas in the disk is

$$M_{\text{HI}} = 2\pi \int_0^{R_{\text{HII}}} (\Sigma(R) - \Sigma_{\text{HII}}) R dR, \quad (2)$$

where R_{HII} is the edge of the HI disk ($\Sigma(R_{\text{HII}}) = \Sigma_{\text{HII}}$). The minus Σ_{HII} term under the integral in Equation (2) appears because both sides of the disk are exposed to the ionizing radiation, and hence each side has an ionized layer of thickness $\Sigma_{\text{HII}}/2$. Integral 2 can be easily taken, so that the fraction of the disk that is neutral is

$$f_{\text{HI}} = \frac{M_{\text{HI}}}{\nu M_{200}} = 1 - \frac{\Sigma_{\text{HII}}}{\Sigma_0} \left(1 + \ln \frac{\Sigma_0}{\Sigma_{\text{HII}}} + \frac{1}{2} \left(\ln \frac{\Sigma_0}{\Sigma_{\text{HII}}} \right)^2 \right). \quad (3)$$

⁴ I also notice that several recent studies of the photoionization effect that did not treat the radiative transfer of ionizing radiation (Hoeft et al. 2006; Crain et al. 2007; Okamoto et al. 2008) found that the best-fit value of $\alpha = 2$. However, in the simulations with the full spatially-variable and time-dependent 3D radiative transfer we always find that the best-fit value of α is 1, even in simulations run with widely different codes, like the moving mesh code of Gnedin (1995) and the currently used ART code.

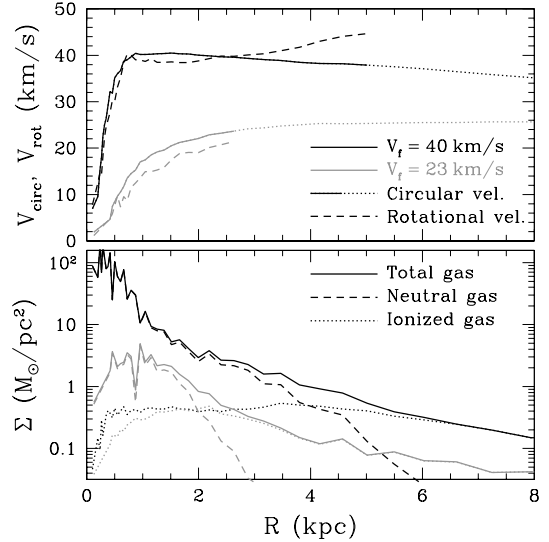


FIG. 3.— The circular and rotational velocity profiles (top) and surface density profiles for the total, ionized, and neutral gas (bottom) for two model galaxies at $z=0$, one with $V_f = 40$ km/s (black lines) and another one with $V_f = 23$ km/s (gray lines; the lowest of two black symbols at this velocity in Figures 1 and 2). In the circular velocity plot, the solid segment of the circular velocity shows its extent over the HI disk, whereas the dotted line shows the extension of the line into the region where there is no atomic gas.

This dependence (for the combination $\nu/\mu^2 = 8$, which is somewhat on a lower side but still plausible, and $\Sigma_{\text{HII}} = 0.4 M_{\odot}/\text{pc}^2$ - the reason for the latter choice will become clear below⁵), multiplied by Equation (1) and plotted as a function of V_{max} , is shown in Figure 2 with the dashed line. It does not fit the simulation results perfectly, but roughly traces the lower envelope of filled symbols; this simplistic model does not account for stellar contribution to the observed BTFR, and is therefore can only serve as an approximation to the lower limit of the observed baryonic fraction of model galaxies.

From an observational perspective, it may be useful to know what fraction of the ionized gas is actually inside the HI disk. In the simple model this quantity is easy to compute,

$$M_{\text{HII}}(R < R_{\text{HII}}) = 2\pi \int_0^{R_{\text{HII}}} \Sigma_{\text{HII}} R dR,$$

or

$$f_{\text{HII}}(R < R_{\text{HII}}) = \frac{M_{\text{HII}}(R < R_{\text{HII}})}{\nu M_{200}} = \frac{1}{2} \frac{\Sigma_{\text{HII}}}{\Sigma_0} \left(\ln \frac{\Sigma_0}{\Sigma_{\text{HII}}} \right)^2. \quad (4)$$

The fraction of ionized gas outside the HI disk is then simply one minus the sum of Equations (3) and Equation (4). The long-dashed line in Figure 2 shows Equation (4) as a function of V_{max} . The ionized gas starts dominating the disk mass only for $V_{\text{max}} < 30$ km/s, but makes a $> 20\%$ contribution all the way to $V_{\text{max}} \approx 100$ km/s.

Finally, one may ask where the ionized gas, apparent in Figures 1 and 2, is actually located in model galaxies? To answer that question, I show in Figure 3 surface density profiles for the total, ionized, and neutral (atomic and molecular, although the molecular fraction in the shown galaxies is small) gas in two galaxies, in which the ionized gas contribution is large. In both galaxies neutral gas forms an approximately exponential disk, while the surface density of the ionized com-

⁵ This is also the column density of a typical sub-DLA absorption system.

ponent remains approximately constant well outside the scale length of the neutral disk. These trends are consistent with the simple analytical model presented above. The choice of $\Sigma_{\text{HII}} = 0.4 M_{\odot} / \text{pc}^2$ is the actual value of the fixed surface density of the ionized gas found in the simulation.

The top panel of Fig. 3 also shows the circular velocity profiles for the two galaxies and the rotational velocity of HI gas. The difference between the two is due to non-circular motions in the gas; this difference is consistent with the prior theoretical models (Valenzuela et al. 2007; Dalcanton & Stilp 2010; Trujillo-Gomez et al. 2011) and observational measurements of galactic rotation curves (c.f. Trachternach et al. 2008; Adams et al. 2011).

4. CONCLUSIONS

The baryonic Tully-Fisher relation is an important observational constraint on cosmological and galactic models. However, it is critical to keep in mind that in observations only stars, molecular, and atomic gas are counted, while the contribution of the ionized gas is almost universally missed. Hence the observed BTFR does not count *all baryons*. Comparison of such observations to theoretical predictions is, therefore, highly non-trivial, and requires a proper modeling of radiative transfer of ionizing radiation, at least in an approximate form.

In this paper I present an example of such modeling in the form of a cosmological numerical simulation with radiative transfer. The simulation is not fully realistic, since it does not include a treatment of supernova feedback, and thus overestimates the baryonic fraction of model galaxies. Even with this incomplete treatment, low mass model galaxies contain large, and for $V_f \lesssim 50 \text{ km/s}$ dominant, contribution of ionized gas.

The ionized gas is present in the gaseous disks of model galaxies in two regions: the outer parts of the disks are ion-

ized since their surface densities (and, hence, column densities) are too low. Even more importantly, the outer layers of the inner disks are also ionized, because they are exposed to the cosmic ionizing background and to the stellar radiation that manages to escape from the central regions of the galactic disks into their outer layers. These layers are direct analogs of the Reynolds' layer observed in the Milky Way galaxy (Reynolds 1993), but their relative contribution to the total mass budget becomes progressively larger as galactic disks become less massive, less dense, and allow ionizing radiation to reach deeper.

The existence of this ionized gas is not just a theoretical conjecture - it is unavoidable from purely physical grounds, since the cosmic ionizing background must ionize the outer layers of galactic HI disks (on both sides) down to column densities of Lyman Limit systems, $N_{\text{HI}} \gtrsim 10^{19} \text{ cm}^{-2}$ (in my simulation it is $\Sigma_{\text{HII}} = 0.2 M_{\odot} / \text{pc}^2$ or, equivalently, $\text{HI} = 2.5 \times 10^{19} \text{ cm}^{-2}$).

I am grateful to Andrey Kravtsov for enlightening discussions and constructive criticism. Throughout the stormy refereeing process, different referees offered constructive and not-so-constructive criticisms. I am grateful to all of them, as the final manuscript ended up being a major improvement over the original draft. This work was supported in part by the DOE at Fermilab, by the NSF grant AST-0908063, and by the NASA grant NNX-09AJ54G. The simulations used in this work have been performed on the Joint Fermilab - KICP Supercomputing Cluster, supported by grants from Fermilab, Kavli Institute for Cosmological Physics, and the University of Chicago. This work made extensive use of the NASA Astrophysics Data System and arXiv.org preprint server.

REFERENCES

- Adams, J. J., Gebhardt, K., Blanc, G. A., Fabricius, M. H., Hill, G. J., Murphy, J. D., van den Bosch, R. C. E., & van de Ven, G. 2011, ArXiv e-prints
- Begum, A., Chengalur, J. N., Karachentsev, I. D., & Sharina, M. E. 2008, MNRAS, 386, 138
- Bell, E. F. & de Jong, R. S. 2001, ApJ, 550, 212
- Crain, R. A., Eke, V. R., Frenk, C. S., Jenkins, A., McCarthy, I. G., Navarro, J. F., & Pearce, F. R. 2007, MNRAS, 377, 41
- Dalcanton, J. J. & Stilp, A. M. 2010, ApJ, 721, 547
- Dutton, A. A. & van den Bosch, F. C. 2009, MNRAS, 396, 141
- Freeman, K. C. 1999, in Astronomical Society of the Pacific Conference Series, Vol. 170, The Low Surface Brightness Universe, ed. J. I. Davies, C. Impey, & S. Phillips, 3–
- Gnedin, N. Y. 1995, ApJS, 97, 231
- . 2000, ApJ, 535, L75
- Gnedin, N. Y. & Abel, T. 2001, New Astronomy, 6, 437
- Gnedin, N. Y. & Kravtsov, A. V. 2010, ApJ, 714, 287
- Gurovich, S., Freeman, K., Jerjen, H., Staveley-Smith, L., & Puerari, I. 2010, AJ, 140, 663
- Gurovich, S., McGaugh, S. S., Freeman, K. C., Jerjen, H., Staveley-Smith, L., & De Blok, W. J. G. 2004, PASA, 21, 412
- Haardt, F. & Madau, P. 2001, in Clusters of Galaxies and the High Redshift Universe Observed in X-rays, ed. D. M. Neumann & J. T. V. Tran
- Hoefl, M., Yepes, G., Gottlöber, S., & Springel, V. 2006, MNRAS, 371, 401
- Kravtsov, A. V. 1999, PhD thesis, New Mexico State University
- Kravtsov, A. V., Klypin, A., & Hoffman, Y. 2002, ApJ, 571, 563
- Krumholz, M. R. & Tan, J. C. 2007, ApJ, 654, 304
- Marín, F. A., Gnedin, N. Y., Seo, H.-J., & Vallinotto, A. 2010, ApJ, 718, 972
- McGaugh, S. 2011, ArXiv e-prints
- McGaugh, S. S. 2005, ApJ, 632, 859
- McGaugh, S. S., Schombert, J. M., Bothun, G. D., & de Blok, W. J. G. 2000, ApJ, 533, L99
- McGaugh, S. S. & Wolf, J. 2010, ApJ, 722, 248
- Mo, H. J., Mao, S., & White, S. D. M. 1998, MNRAS, 295, 319
- Okamoto, T., Gao, L., & Theuns, T. 2008, MNRAS, 390, 920
- Pfenniger, D. & Revaz, Y. 2005, A&A, 431, 511
- Prada, F., Klypin, A. A., Cuesta, A. J., Betancort-Rijo, J. E., & Primack, J. 2011, ArXiv e-prints
- Reynolds, R. J. 1993, in American Institute of Physics Conference Series, Vol. 278, Back to the Galaxy, ed. S. S. Holt & F. Verter, 156–165
- Rudd, D. H., Zentner, A. R., & Kravtsov, A. V. 2008, ApJ, 672, 19
- Stark, D. V., McGaugh, S. S., & Swaters, R. A. 2009, AJ, 138, 392
- Torres-Flores, S., Epinat, B., Amram, P., Plana, H., & Mendes de Oliveira, C. 2011, ArXiv e-prints
- Trachternach, C., de Blok, W. J. G., McGaugh, S. S., van der Hulst, J. M., & Dettmar, R.-J. 2009, A&A, 505, 577
- Trachternach, C., de Blok, W. J. G., Walter, F., Brinks, E., & Kennicutt, Jr., R. C. 2008, AJ, 136, 2720
- Trujillo-Gomez, S., Klypin, A., Primack, J., & Romanowsky, A. J. 2011, ApJ, 742, 16
- Tully, R. B. & Fisher, J. R. 1977, A&A, 54, 661
- Valenzuela, O., Rhee, G., Klypin, A., Governato, F., Stinson, G., Quinn, T., & Wadsley, J. 2007, ApJ, 657, 773
- Verheijen, M. A. W. 2001, ApJ, 563, 694
- Zwaan, M. A., Meyer, M. J., Staveley-Smith, L., & Webster, R. L. 2005, MNRAS, 359, L30